Available online at www.sciencedirect.com
ScienceDirect
Acta Materialia 57 (2009) 2576–2582
Acta MATERIALIA
www.elsevier.com/locate/actamat

Size-effect on stress behavior of the AlN/TiN film

D. Chen, Y.M. Wang, X.L. Ma *

Shenyang National Laboratory for Materials Science, Institute of Metal Research, Chinese Academy of Sciences, Wenhua Road 72, Liaoning, Shenyang 110016, China

Received 22 October 2008; received in revised form 9 February 2009; accepted 9 February 2009
Available online 13 March 2009

Abstract

The stress behavior of AlN/TiN superlattice film has been studied by means of a crystal-chemical atomic dynamics simulation based on first-principles calculations. The size-effects on stress behavior are demonstrated and discussed in detail. Stress behavior depends not only on AlN thickness but also on structural relaxation and strain distribution in the film. When the AlN thickness exceeds a critical one, the superlattice film is metastable. Stress behavior can be traced to the AlN/TiN interface structure and its variation with strain relaxation, which may reflect the main strain characteristics caused by AlN structural transformation in this film.
© 2009 Acta Materialia Inc. Published by Elsevier Ltd. All rights reserved.

Keywords: Superlattice; Stress; Transformation; Simulation

1. Introduction

The epitaxial stabilization of nonequilibrium structures has been widely studied due to the promising mechanical and chemical properties of multilayer thin films [1–8]. The stabilization of epitaxial metastable film is determined by its composition, crystallographic structure and interface structure, which are closely related to the properties of superlattices used in device technology [9–10]. AlN/TiN films are of theoretical and experimental interest because their physical properties are important for applications in microelectronic devices, protective coatings of cutting tools and other mechanical components. At ambient temperature and pressure, AlN has a wurtzite structure (*w*-AlN). However, cubic AlN (B1-AlN) can be synthesized under high pressures of more than 22.9 GPa [11] or epitaxially stabilized in a superlattice film [2–8]. In Ref. [12], we have simulated the stability of such cubic B1-AlN using a AlN/TiN(001) superlattice model and reported that the cubic B1-AlN will be transformed to hexagonal *w*-AlN once the AlN thickness is beyond a critical one (~1.95 nm), later Ref. [13] provided further experimental support for this finding. In fact, the growth of thin or superlattice film is of great relevance to its specific physical and chemical properties. For example, once the AlN layer in AlN/TiN film exceeds a critical thickness, the strain in cubic AlN is relieved by the formation of hexagonal AlN. Therefore, its physical and chemical properties might be changed due to the strain relaxation caused by the AlN structural transformation. As we know, a superlattice is a complicated system with multiple degrees of freedom, including the number of layers, the number of dimensions and the individual layer strain within it. Although many studies [14–19] have revealed that strain plays a fundamental role in determining structural properties of superlattice film, how the strain is relaxed and then distributed in a superlattice film remains unclear. In addition, Sander et al. [20,21] have observed that the surface stress varies in an oscillatory way during the epitaxial growth of Co and FeMn on Cu(001). However, to the best of our knowledge, no reports exist about the epitaxial growth behavior of superlattice. In this paper, we have demonstrated the size-effects on the stress behavior of the AlN/TiN superlattice and then evaluated the new strain distribution in the superlattice caused by AlN structural transformation using crystal-chemical atomic dynamics simulation based on

* Corresponding author.
E-mail address: xlma@imr.ac.cn (X.L. Ma).

1359-6454/$36.00 © 2009 Acta Materialia Inc. Published by Elsevier Ltd. All rights reserved.
doi:10.1016/j.actamat.2009.02.018

first-principles calculations. This study provides some useful fundamental information on establishing the relationship between physical (and chemical) property and the size-effect of low-dimensional nanomaterials.

2. Radial distribution function

As shown in Fig. 1 (Fig. 2 in Ref. [12]), an initial B1-AlN/TiN(001) superlattice cell was constructed based on the first-principles results [22]. To simulate the pseudomorphic growth and structural transformation, the B1-AlN layers were confined in the TiN(001) substrate in which the coherent interface is kept. The simulation of the B1-AlN/TiN(001) superlattice cell was implemented by means of the Aix-la-Chapelle's crystal-chemical atomic dynamics (aixCCAD) method [23–25], which can give a direct access to the atomic trajectories and details of AlN structural information on an atomic level. In the calculations, the number of AlN layers was variable in the AlN/TiN superlattice cell. All simulations were performed for the case of an NVT ensemble, whereby the number of particles N, the volume V and the temperature T can be set to desired values. The interatomic forces for determining the relaxed atomic positions were calculated by the velocity Verlet algorithm [26]. The summation over the Coulomb interactions was done using the Ewald summation technique [27]. The convergence parameter was set to 0 and the largest reciprocal space vector k_{max} to 4.5 $Å^{-1}$. A cut-off radius of 6.0 Å turned out to be appropriate with respect to both speed and accuracy. To ensure a full relaxation for each mode with the H2 regions of 3, 7 and 11 monolayers (MLs), the time step chosen was 0.001 ps and the total simulation time was up to 300,000 time steps.

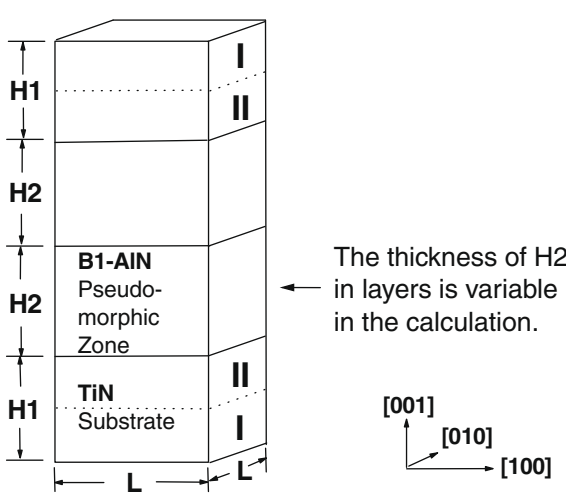

Fig. 1. Scheme of the B1-AlN/TiN(001) superlattice cell (Fig. 2 in Ref. [12]). Each H1 zone has 6-monolayer (ML) TiN in which 3-ML is designated bulk-like (H1 I) for TiN substrate and all atoms in it are fixed; another three MLs are close to the interface (H1 II) in which the atoms can be relaxed. The H2 + H2 zone of B1-AlN with a variable number of layers is confined by the two H1. The size of the initial supercell is L × L × (2H1 + 2H2) $Å^3$.

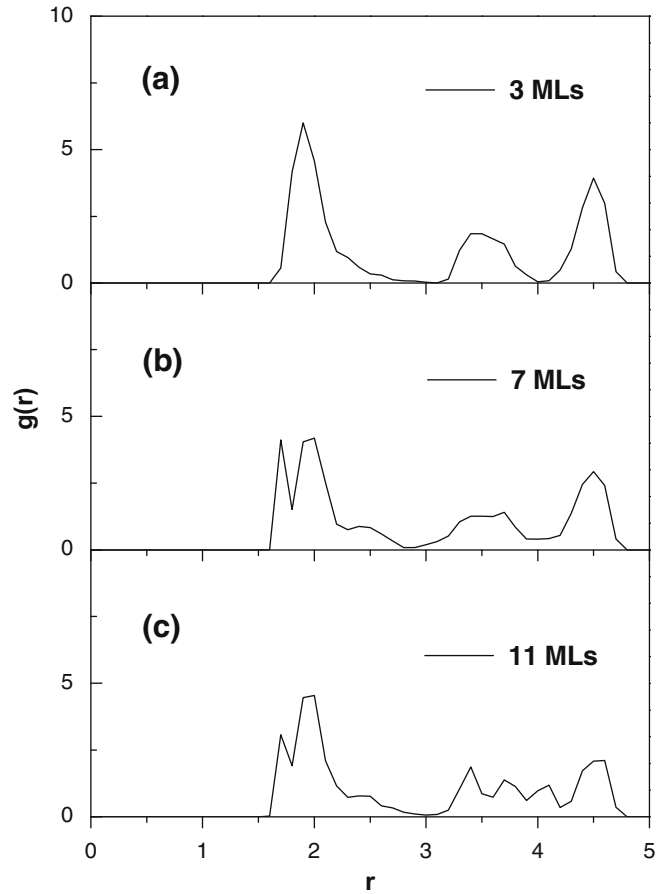

Fig. 2. Radial distribution functions (g(r)) of AlN in the AlN/TiN(001) superlattice cell for 3, 7 and 11 ML AlN, respectively. The interatomic separation, r, is in Å.

For ionic crystals, the long-range interaction can be described in terms of the Coulomb interaction potential, while the short-range interaction is expressed by the Pauli repulsive potential. The potential function is given in Refs. [23–25]. In the calculation, the bond length–bond strength parameter r_0 was respectively taken as 1.786 Å for w-AlN [25] and 1.856 Å for TiN [12]. To describe the AlN atomic arrangement and structural information for variational AlN layers, the radial distribution functions (RDFs) were calculated for AlN in the AlN/TiN cell. More details of the simulation method and the parameters of the potentials chosen can be found elsewhere [12].

In Fig. 2, we show the RDF results of AlN in the B1-AlN/TiN(001) superlattice cell when AlN layer includes 3, 7, or 11 MLs, respectively. In Fig. 2a, for 3-ML AlN, it is clearly shown that there are three peaks in the RDF, reflecting the fact that the AlN region maintains the characteristics of the cubic structure. In Fig. 2b, for 7-ML AlN, one RDF peak is split and other two peaks are slightly broadened, which indicates that there is a small deformation in the cubic AlN region. In Fig. 2c, for 11-ML AlN, the RDF peaks are very different from Fig. 2a and b: they are split into several conjunctive and widened ones. In this case, the crystallinity of the cubic

structure has completely deteriorated and the hexagonal structure has been formed in the AlN region.

In the cubic AlN region of the AlN/TiN cell, each Al atom has an octahedral environment with 6 N atoms. In the hexagonal AlN, each Al atom has 4 N nearest-neighbor atoms. After the AlN structural transformation, the coordination number in the AlN region will be changed from 6 to 4. For 3-ML and 7-ML AlN, as plotted in Fig. 2a and b, the cubic structure is the characteristic of AlN region. Once the AlN thickness is increased to 11-ML beyond its critical one, ~1.95 nm (~9.5 MLs) [12], the RDF in Fig. 2c quite like wurtzite *w*-AlN in Refs. [28,29], suggesting that the hexagonal structure is dominant in the AlN region. Fig. 2 shows that strain exists in the AlN/TiN superlattice cell in the structural transformation from cubic to hexagonal AlN.

3. Results and discussion

3.1. Stress oscillation

To reveal the size-effects on the stress behavior of AlN/TiN superlattice and to understand more deeply the relationship between the strain distribution and the formation of hexagonal AlN, one approach is to simulate the structural variation with stress relaxation at different AlN thicknesses, as we have done for 3, 7 and 11 ML AlN layers.

Fig. 3 shows the time evolutions of (total atomic level) stress for a 3-ML AlN layer along the [100], [010] and [001] directions, respectively. At a certain time step, the stress of each direction is defined as the summation of the force acting on every atom along this direction in the AlN/TiN cell.

In Fig. 3, all the stress curves can be divided into three stages according to their oscillation properties, which are sensitive to the new strain distribution after the AlN/TiN cell is relaxed at different time steps. Arrows (1) and (2) point to the positions from which the oscillation trends of stress begin to change noticeably. In the first stage, from 0 to position (1) (12,000 time steps), the stress curve along the [001] direction oscillates around the abscissa, but the ones along the [100] and [010] directions barely oscillate. In the second stage, from position (1) to position (2) (100,000 time steps), oscillations along the [100] and [010] directions have become obvious, and their average values are approximately 0. In the last stage, from position (2) to the end of the simulation (300,000 time steps), the oscillation modes are different: although the curves along the [010], [001] and [001] directions oscillate around their respective average oscillation values, the value is negative (compressive) for [010] but positive (tensile) for [001] and [100], and the average value is larger along the [001] direction than along the [100] direction.

For a 7-ML AlN layer (Fig. 4), the curves are also separated into three stages. In stage 1, from 0 to position (1) (19,000 time steps), each curve is similar to that in Fig. 3. In stage 2, from position (1) to position (2) (100,000 time steps), the stress along the [001] direction has a positive average oscillation value, but those along the [100] and [010] directions have negative values. In the last stage, from position (2) to the end of the simulation, it is noticeable that the average oscillation value along the [100] direction tends to negative, but is positive at the same stage shown in Fig. 3.

Fig. 5 shows the stress curves for a 11-ML AlN layer, in which the AlN thickness has exceeded its critical value (~9.5 MLs) [12]. In this case, the stress oscillation

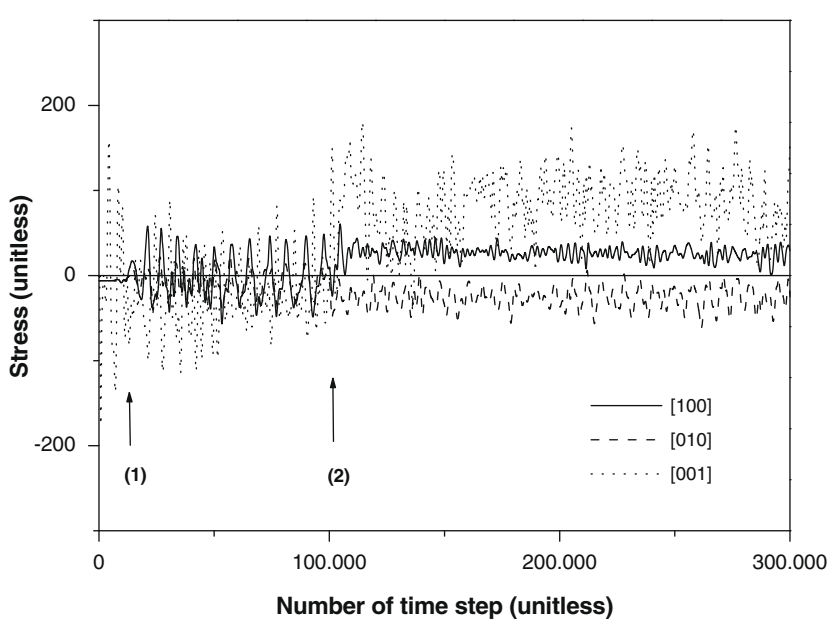

Fig. 3. Time evolutions of stress for a 3-ML AlN layer along the [100], [010] and [001] directions.

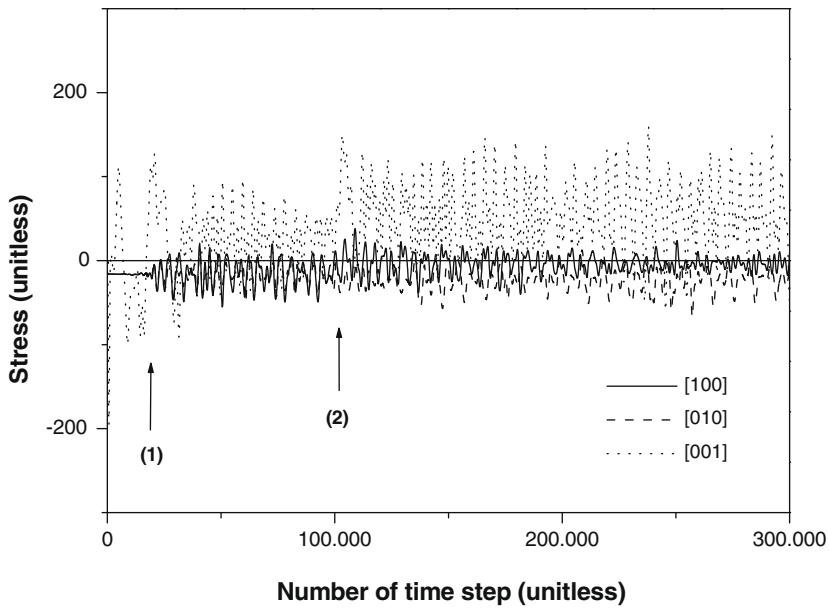

Fig. 4. Time evolutions of stress for a 7-ML AlN layer along the [100], [010] and [001] directions.

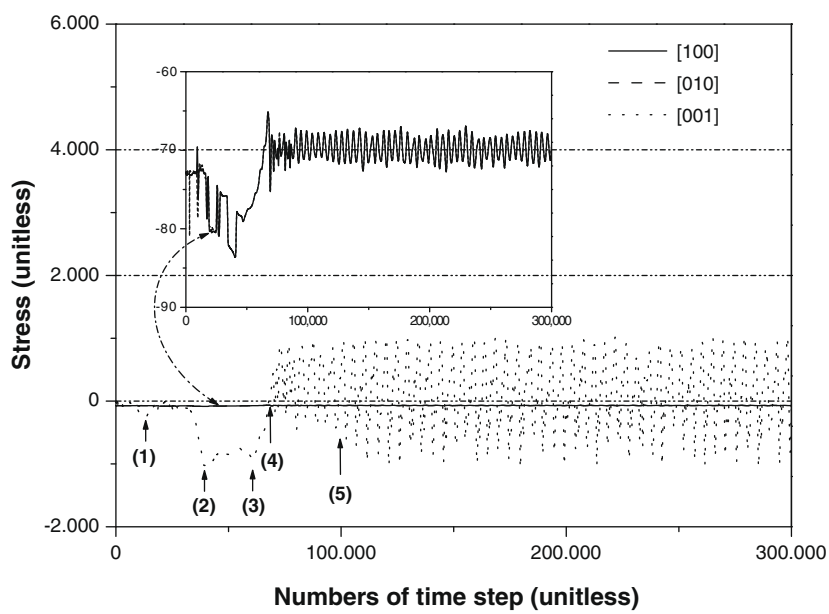

Fig. 5. Time evolutions of stress for a 11-ML AlN layer along the [100], [010] and [001] directions.

amplitudes along the [100] and [010] directions become much smaller than that along the [001] direction. As shown in the inset of Fig. 5, they almost overlap and their average oscillation values are both negative.

Compared with Figs. 3 and 4, there is a significant stress change along the [001] direction in Fig. 5, i.e. a strain barrier caused by AlN structural transformation appears along the [001] direction.

In summary, we mark five positions (1)–(5) in Fig. 5. From 0 to position (1) (8000 time steps), the stress curve goes down to the first negative minimum at position (1), at this point the AlN region still maintains the cubic structure but has a small deformation. In this case, the only stress at the interface is compressive. From position (1) to position (2) (41,000 time steps), most of the AlN layer is in the compressive stress due to insufficient compensation of strain energy in the AlN/TiN superlattice by the bulk energy of cubic AlN. At position (2), the curve comes to its second negative minimum, lower than the first one. At this time, most of the AlN layer has been deformed. From position (2) to position (3) (61,000 time steps), the curve is approximately a plateau. Position (3) is at the end of this plateau with the third negative minimum. This indicates that the AlN structural transformation has been completed under the compressive stress before the end of the plateau. Then, the curve goes rapidly up and crosses the zero level at

position (4) (70,000 time steps). The curve variation from (1) to (4) indicates that the AlN structural transformation is caused by compressive stress.

From position (4) to position (5) (100,000 time steps), the average oscillation value is positive but decreases with time. At position (4), the hexagonal structure is dominant in the AlN region, and most of atomic kinetic energy has been already converted into potential energy of the AlN/TiN superlattice cell. The tensile stress is produced with the formation of hexagonal AlN in the AlN/TiN cell. At position (5), the AlN structural transformation has finished.

In the last stage, from position (5) to the end of the simulation, the average oscillation value tends to zero. This characteristic is mainly due to the formation of hexagonal AlN structure, since there is only a very small total energy difference (less than 1.3%) between the 100,000 and 300,000 time steps. This demonstrates that the hexagonal AlN structure would be stable in this stage.

In Fig. 5, there are three basic stages during the whole evolution of stress. (a) From 0 to position (4), the AlN structural transformation proceeds since the compressive strain energy in the AlN/TiN superlattice is larger and difficult for the bulk energy of cubic AlN to compensated for. (b) From position (4) to position (5), the tensile stress is dominant owing to the formation of hexagonal AlN structure. (c) From position (5) to the end of the simulation, the stress varies periodically and its average value is approximately equal to zero. The complete formation of stable hexagonal AlN means that the chosen 300,000 time-step is long enough to simulate AlN structural transformation.

3.2. Strain distribution

In general, the stability of an interface configuration is mainly determined by its energy. The smaller the interface energy, the more stable the interface structure. It can be expected that in AlN/TiN superlattice after structure transformation, the interface energy and interface spacing would be increased due to the larger lattice mismatch between hexagonal AlN and cubic TiN. In experiments, the interface energy is hardly accessible and might be affected by deposition techniques, temperatures and process conditions [2–8]. We use the first-principles plane-wave pseudopotential (PWPP) method [30] to calculate the interface energies of the initial AlN/TiN configuration (at 0 time step) and the final AlN/TiN configuration (at the end of the simulation) in Fig. 5 by calculating the total energy after structural relaxation. The computational details and the equations used to calculate the interface energy are given in our previous work [22]. In this study, we find that the calculated interface energy of the initial AlN/TiN configuration is only 0.775 J m^{-2}, much smaller than that of the final one (3.622 J m^{-2}). We attribute this to the change in interfacial atomic bonding between AlN and TiN caused by the AlN structure transformation, i.e. with this transformation the interface energy of AlN/TiN becomes larger and larger, and finally the interface energy of the final AlN/TiN configuration is higher than that of the initial one. In what follows, we will explain this phenomenon qualitatively.

We define the bulk energy of cubic AlN as $E_{B1\text{-}AlN}$, the strain energy of the AlN layer caused by the B1-AlN/TiN interface mismatch as $E^{strain}_{B1\text{-}AlN}$, and the interface energy as E_{Inter}. Thus, as mentioned in Section 3.1 of Ref. [12], the following inequality describing the structure transformation from cubic to hexagonal AlN can be obtained:

$$E^{strain}_{B1\text{-}AlN} + E_{Inter} < E_{w\text{-}AlN} - E_{B1\text{-}AlN}, \quad (1)$$

where $E_{w\text{-}AlN}$ is the bulk energy of hexagonal AlN. From Eq. (1), when the sum of $E^{strain}_{B1\text{-}AlN}$ and E_{Inter} becomes smaller than a constant value of $E_{w\text{-}AlN} - E_{B1\text{-}AlN}$ with the AlN thickness exceeding its critical value, ~1.95 nm (~9.5 MLs), the structural transformation will take place.

The $E^{strain}_{B1\text{-}AlN}$ of the initial AlN/TiN configuration is maximum and E_{Inter} is minimum after relaxation. As hexagonal AlN forms, $E^{strain}_{B1\text{-}AlN}$ is reduced but E_{Inter} increases. However, after structural transformation, the $E^{strain}_{B1\text{-}AlN}$ of the final AlN/TiN configuration will be minimum and E_{Inter} maximum. To evaluate the stability of the AlN/TiN superlattice cell, we should consider not only the interface energy value itself but also changes in the strain energy and interface energy with structural transformation. The AlN/TiN cell with hexagonal AlN would be stable if it meets the energy criteria of inequality (1). Although the results are from the AlN/TiN system, we expect this energy criteria would also be appropriate for other superlattice systems.

In the whole evolution of relaxation, the inequality (1) should be satisfied no matter how the AlN structure is transformed in the AlN/TiN superlattice. However, the rate of decrease of $E^{strain}_{B1\text{-}AlN}$ should at least be larger than the rate of increase of E_{Inter}. Only in this case is the maximum reduction in $E^{strain}_{B1\text{-}AlN}$ able to compensate the energy consumed by the formation of AlN hexagonal structure. Usually, it is very difficult to accurately describe the strain distribution in the superlattice. However, from the above qualitative analysis, we can evaluate the strain distribution within the superlattice cell of the final AlN/TiN configuration: the strains are not uniformly distributed and the greatest strains are concentrated in the vicinity of the interface. This is the main reason why a close relationship exists between strain distribution and interface structure.

Fig. 6 shows the final atomic configuration of hexagonal AlN on TiN substrate after 300,000 time steps. Fig. 6a is a projection along the $[0\,1\,0]_{TiN}$ direction and Fig. 6b is a view along the $[1\,\bar{1}\,0]_{TiN}/[1\,\bar{2}\,1\,0]_{AlN}$ (Fig. 4e in Ref. [12]). An observable deformation around the interface is attributed to a strain concentration around this interface.

The final AlN/TiN atomic configuration in Fig. 6 looks at first sight like the interface structural models proposed by Ma et al. (models III and IV in Ref. [31]). In fact, there are two differences between them: (1) there is a deformation around the interface in Fig. 6 but no deformation in the Ref. [31] models; (2) models III and IV are distinguished

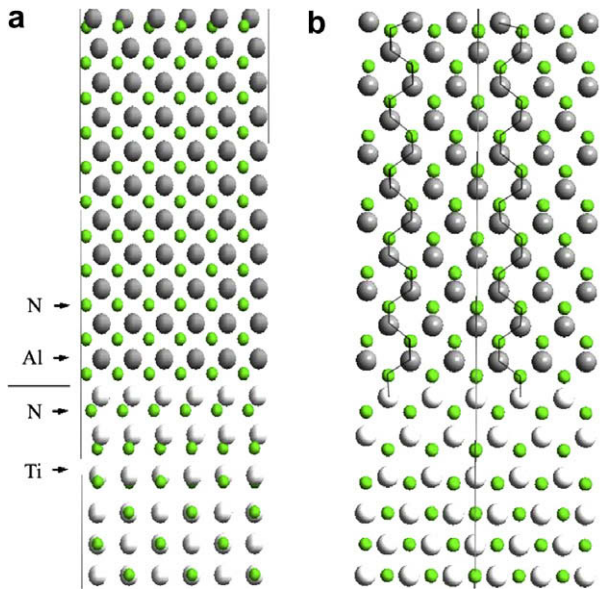

Fig. 6. Schematic of the final AlN/TiN configuration: (a) is projected along the $[010]_{TiN}$ direction, and (b) is viewed along $[1\bar{1}0]_{TiN}/[1\bar{2}10]_{AlN}$ (Fig. 4e in Ref. [12]).

by N atoms of different sublayers in the unit cell of ideal *w*-AlN in Ref. [31]. However, in Fig. 6b, if looking at the atoms along the left zigzag line in the AlN region, the final AlN/TiN configuration looks similar to model III; if looking at the atoms along the right zigzag line, the final configuration resembles model IV. Therefore, strictly speaking, the AlN structure shown in Fig. 6 is not an ideal wurtzite-type crystallite, in which incomplete strains still exist. After the AlN structural transformation, great strains determine the atomic positions around the interface and result in atomic deviations in the vicinity of the interface. In this paper, the stress is defined as the total force on every atomic position at a certain time step. Accordingly, the stress behavior is closely related to the stress variation of each atom in the AlN/TiN cell. Since strain concentration exists in the vicinity of the interface, it can be expected that the stress behavior should be mainly determined by the interface structure and its variation in strain relaxation.

Although the stress behavior in AlN/TiN superlattice is complicated, our results provide fundamental insights into it. In the following, we compare the stress behaviors in the last evolution stage shown in Figs. 3–5, which show that these behaviors depend strongly on the AlN thickness in the AlN/TiN cell. When it is 3-MLs, the AlN region retains the characteristics of the cubic structure and the strain around the interface is very small. The average oscillation value for each curve in Fig. 3 is different but has the nearly same oscillation amplitude. When the AlN is 7-MLs, a small deformation will occur in the cubic AlN region. In Fig. 4, the stresses along the [100] and [010] directions are different, and the stress oscillation amplitude along the [001] direction is relatively larger than those along [100] and [010]. In these two cases, the AlN thickness is below its critical one (~9.5 MLs [12]), and the superlattice is metastable. When the AlN thickness reaches 11-MLs, AlN structural transformation takes place, and the interface energy and strain in the vicinity of the interface increase greatly. As shown in Fig. 5, the stress oscillation amplitude along the [001] direction is pronounced. The atomic dynamics relaxation step in this study is an iterative process in which the coordinates of atoms and possibly the computational cell parameters are adjusted so that the total energy of the structure is reduced to a minimum. Each computational cell has been fully relaxed, not only in the [001] direction but also with lateral flexibility of atoms along the [100] and [010] directions. However, it can be found that after relaxation the atomic movements are significantly different in the three spatial directions. With the AlN structure transforming, to stabilize the hexagonal AlN structure the atomic movements along the [001] direction are much larger in magnitude than those along the [100] and [010] directions, and atomic bonding would change near the interface in the AlN/TiN cell. As a result, it appears that the stress behavior of the AlN/TiN cell is mainly determined by the stress along the [001] direction and it would display a strong dependence on AlN thickness and interface structure. Overall, the stress behavior is traced to the AlN structure, interface structure and its response to strain in the AlN/TiN superlattice cell. Therefore, stress behavior depends not only on AlN thickness but also on structural relaxation and strain distribution in the AlN/TiN superlattice.

Recently, Sander et al. [20,21] have reported that the oscillatory phenomenon of surface stress was observed during epitaxial growth of Co and FeMn on Cu(001). Our results indicate that it also exists in the formation of a superlattice and its interface structure would be determined by strain relaxation in the superlattice. This study is preliminary to gaining an understanding of the stress behavior in the AlN/TiN superlattice.

4. Conclusions

We have studied the size-effects on stress behavior in the AlN/TiN superlattice by applying a crystal-chemical atomic dynamics simulation based on first-principles calculations. Stress behavior depends not only on AlN thickness but also on structural relaxation and strain distribution. When the AlN thickness exceeds a critical, the AlN structural transformation takes place. The strains in the superlattice are not uniformly distributed after relaxation and the greatest strain is concentrated in the vicinity of the interface. From the final stress evolution stage shown in Fig. 5, we can conclude that the stress behavior is closely connected with the interface structure and its variation with strain relaxation in the AlN/TiN superlattice.

Acknowledgments

We sincerely thank Dr. Bernhard Eck, Institute of Inorganic Chemistry, Aachen University of Technology

(RWTH), Germany, for his valuable help in performing the calculations using the aixCCAD program. This work was supported by the National Basic Research Program of China (2002CB613503 and 2009CB623705).

References

[1] Vepek S, Vepek-Heijman MGJ, Karvankova P, Prochazka J. Thin Solid Films 2005;476:2.
[2] Madan A, Kim IW, Cheng SC, Yashar P, Dravid VP, Barnett SA. Phys Rev Lett 1997;78:1743.
[3] Yashar P, Chu X, Barnett SA, Rechner J, Wang YY, Wong MS, et al. Appl Phys Lett 1998;72:987.
[4] Kim IW, Li Q, Marks LD, Barnett SA. Appl Phys Lett 2001;78:892.
[5] Pankov V, Evstigneev M, Prince RH. Appl Phys Lett 2002;80:4142.
[6] Pankov V, Evstigneev M, Prince RH. J Appl Phys 2002;92:4255.
[7] Li Q, Kim IW, Barnett SA, Marks LD. J Mater Res 2002;17:1224.
[8] Li G, Lao J, Tian J, Han Z, Gu M. J Appl Phys 2004;95:92.
[9] Söderberg H, Odén M, Molina JM, Hultman L. J Appl Phys 2005;97:114327.
[10] Schuster E, Keune W, Reuter D, Westerholt K. Superlattices Microstruct 2005;37:313.
[11] Ueno M, Onodera A, Shimomura O, Takemura K. Phys Rev B 1992;45:10123.
[12] Chen D, Ma XL, Wang YM. Acta Mater 2005;53:5223.
[13] Karimi A, Allidi G, Sanjines R. Surf Coat Technol 2006;201:4062.
[14] Snyder CW, Orr BG, Kessler D, Sander LM. Phys Rev Lett 1991;66:3032.
[15] Snyder CW, Orr BG, Munekata H. Appl Phys Lett 1993;62:46.
[16] He XG, Erdtmann M, Williams R, Kim S, Razeghi M. Appl Phys Lett 1994;65:2812.
[17] Giannini C, Tapfer L, Zhuang Y, De Caro L, Marschner T, Stolz W. Phys Rev B 1997;55:5276.
[18] Xu J, Kamiko M, Zhou Y, Yamamoto R, Li G, Gu M. J Appl Phys 2001;89:3674.
[19] Mei FH, Shao N, Dai JW, Li GY. Mater Lett 2004;58:3477.
[20] Sander D, Ouazi S, Stepanyuk VS, Bazhanov DI, Kirschner J. Surf Sci 2002;512:281.
[21] Pan W, Sander D, Lin MT, Kirschner J. Phys Rev B 2003;68:224419.
[22] Chen D, Ma XL, Wang YM, Chen L. Phys Rev B 2004;69:155401.
[23] Dronskowski R, Eck B, Kikkawa S. Jpn J Appl Phys 2000;39:3326.
[24] Eck B, Dronskowski R. J Alloys Comp 2002;338:136.
[25] Eck B, Kurtulus Y, Offermans W, Dronskowski R. J Alloys Comp 2002;338:142.
[26] Swope WC, Andersen HC, Berens PH, Wilson KR. J Chem Phys 1982;76:637.
[27] Ewald PP. Ann Phys 1921;64:253.
[28] Spengler W, Kaiser R, Christensen AN, Muller-Vogt G. Phys Rev B 1978;17:1095.
[29] Cata GF, Lorenzo GR, Odriozola JA, Alvarez LJ. Chem Phys Lett 2002;356:127.
[30] Payne MC, Teter MP, Allan DC, Arias TA, Joannopoulos JD. Rev Mod Phys 1992;64:1045.
[31] Ma XL, Sugawara Y, Shibata N, Ikuhara Y. J Mater Res 1999;14:4685.